IUCr

Acta Crystallographica Section D research papers

Improved estimates of coordinate error for molecular replacement

Robert D Oeffner[a], Gábor Bunkóczi[a], Airlie J McCoy[a] and Randy J Read[a]*

[a]Cambridge Institute for Medical Research, University of Cambridge, Hills Road, Cambridge, Cambridgeshire, CB2 0XY, United Kingdom

Correspondence email: rjr27@cam.ac.uk

Keywords: Phaser, maximum likelihood, molecular replacement

Synopsis

A function for estimating the effective root-mean-square deviation in coordinates between two proteins has been developed that depends on both the sequence identity and the size of the protein and is optimized for use with molecular replacement in *Phaser*. A top peak translation function Z-score over 8 is found to be a reliable metric of when molecular replacement has succeeded.

Abstract

The estimate of the root-mean-square deviation (*RMSD*) in coordinates between the model and the target is an essential parameter for calibrating likelihood functions for molecular replacement (MR). Good estimates of the *RMSD* lead to good estimates of the variance term in the likelihood functions, which increases signal to noise and hence success rates in the MR search. *Phaser* has hitherto used an estimate of the *RMSD* that only depends on the sequence identity between the model and target and which was not optimised for the MR likelihood functions. Variance refinement functionality was added to *Phaser* to enable determination of the effective *RMSD* that optimised the log-likelihood gain (LLG) for a correct MR solution. Variance refinement was subsequently performed on a database of over 21000 MR problems that sampled a range of sequence identities, protein sizes and protein fold classes. Success was monitored with the translation function Z-score (TFZ), where a TFZ of 8 and over for the top peak was found to be a reliable indicator that MR had succeeded for these cases with one molecule in the asymmetric unit. Good estimates of the *RMSD* are correlated with the sequence identity and the protein size. A new estimate of the *RMSD* that uses these two parameters in a function optimized to fit the mean of the refined variance is implemented in *Phaser* and improves MR

outcomes. Perturbing the initial estimate of the *RMSD* from the mean of the distribution in steps of standard deviations of the distribution further increases MR success rates.

1. Introduction

Molecular replacement (MR) (Rossmann & Blow, 1962) relies on the evolutionary principle that two proteins with a high sequence identity are very likely to have similar secondary and tertiary structures and hence low root-mean-square deviation (*RMSD*) in coordinate positions. An estimate of the *RMSD* is an essential parameter used to calibrate likelihood functions in the maximum likelihood approach to MR (Read, 2001). If the estimate is good, then appropriate weight is placed on agreement of reflections at different resolutions and it is not necessary to apply arbitrary resolution cutoffs. However, if the estimate is poor, then the signal is reduced and a correct solution may not be detectable in the MR search.

The *RMSD* is introduced into the likelihood targets via the parameter σ_A.

$$P(E_o; E_c) = \frac{2E_o}{1-\sigma_A^2} \cdot \exp\left(-\frac{E_o^2+\sigma_A^2 E_c^2}{1-\sigma_A^2}\right) \cdot I_0\left(\frac{2E_o E_c}{1-\sigma_A^2}\right) \quad (1)$$

σ_A is a function of resolution (measured by s=1/d, the absolute value of the diffraction vector) that combines the effects of positional errors of the atoms in the model (the *RMSD*) and the completeness of the model f_P, *i.e.* the ratio between the scattering power of the model and of the crystal (Read, 1986) (Srinivasan & Ramachandran, 1966). Ignoring the effects of bulk solvent, σ_A can be expressed in the simple form given in equation (2).

$$\sigma_A = D\sqrt{f_P} \quad (2)$$

where $D = \exp\left(\frac{-2\pi^2}{3} s^2 RMSD^2\right)$ and $f_P = \frac{\Sigma_P}{\Sigma_N}$

To account for defects in the model associated with the lack of bulk solvent, a low resolution falloff is also incorporated in the equation for σ_A.

$$\sigma_A = [1 - k_{sol} exp(-B_{sol} s^2/4)] \cdot D\sqrt{f_p} \quad (3)$$

When an MR calculation is undertaken within the maximum likelihood formalism, σ_A is initialized from estimates of *RMSD* and f_P, typically using generic values for k_{sol} and B_{sol} (McCoy *et al.*, 2007). If the *RMSD* is underestimated σ_A will be overestimated and the log-likelihood gain (LLG) will be smaller than with the correct *RMSD*. Similarly, an overestimate of *RMSD* leads to an underestimate of σ_A and again a reduction in the LLG.

Prior to successful molecular replacement, only the sequence of the target is available to inform the estimation of an appropriate *RMSD* value. Chothia & Lesk (1986) formulated an expression for the relationship between sequence identity and *RMSD* in main-chain atoms based on 32 pairs of homologous structures.

$$RMSD = 0.4e^{1.87H} \text{ Å} \quad (4)$$

where *H* is the fraction of mutated residues between the two sequences. At a sequence identity of 100%, equation (4) has a minimum of 0.4Å. Experiences with a number of test cases (data not shown) indicated that this value was frequently too low for the estimate of the variance term in the maximum likelihood functions as implemented in *Phaser* (McCoy *et al.*, 2007), leading to negative LLG scores, and therefore the formula used in *Phaser* was modified with a lower bound of 0.8Å, which applied in effect above 63% sequence identity. The *RMSD* estimated for the purpose of calculating the variance used in the likelihood function in Phaser (e*RMSD*) was taken as

$$\text{e}RMSD = \max\{0.8, 0.4\, e^{1.87H}\} \quad (5)$$

After the model has been correctly placed, it is possible to refine the *RMSD* parameter that determines σ_A values by maximising the LLG. We term this optimised *RMSD* parameter the variance-RMS (*VRMS*). We anticipated that (4) was sub-optimal for estimating the *VRMS* for four reasons. Firstly, the equation was derived from a very small database of only 32 structures, and they represented a narrow range of comparative lengths of between only 99 and 287 residues. Since the publication of (4) in 1986 the PDB has expanded to include more than 90,000 structures of up to 1500 residues, all potential models for MR. Secondly, unlike the *RMSD*, the *VRMS* is not biased by any explicit atom pair assignment. Thirdly, the actual *RMSD* is not necessarily the best effective *VRMS* to use in the equation for σ_A; the *RMSD* continues to grow dramatically as errors grow, whereas structure factor agreement does not get worse once the error is comparable to the *d*-spacing. Fourthly, we are interested in the best effective *VRMS* to use for the subset of cases for which an MR solution can be found; in the low identity range in particular this will bias *VRMS* to lower values corresponding to models that are better than average. We aimed to find a better initial estimate of *VRMS* from the information available prior to structure solution, namely sequence identity to target, number of residues in the model and fold class. For these reasons, an estimate for the *VRMS* cannot be directly equated with an *RMSD* computed from a structural alignment between two structures. Even if it were possible to obtain a structure-based *RMSD* prior to solving the structure, this *RMSD* would not be as useful as the *VRMS* value that maximises the likelihood in an MR calculation. By the same token, it would be incorrect to employ the *VRMS* for situations when a structure-based *RMSD* value is required.

2. Methods

A database of 21822 MR calculations was generated for optimizing the estimation of the *VRMS*. Computations were performed on an Ubuntu 64-bit queueing system cluster with 5 dual processor quad-core nodes and a total of 320 Gb of memory.

2.1. Target structures

2862 structures were selected from the PDB using the criteria that they were biological monomers, that they had one monomer in the asymmetric unit, and that the associated X-ray data were deposited. Twinned structures were excluded as were structures for which the published R-factor could not be reproduced.

The number of entries in the PDB varies drastically across the range of protein sizes, from very small (fewer than 50 residues) to large (more than 1000 residues). The vast majority of proteins are in the moderate size range of between 100 and 500 residues. Targets were chosen across the range of sizes in the PDB. All PDB structures with 600 residues or more that met the selection criteria were retained, but nonetheless the relatively small number of large structures available limited the quality of the statistics for the largest proteins. The distribution of sizes used is shown in Figure 1a.

Targets were chosen across the range of SCOP classes (Murzin *et al.*, 1995). There are 10 SCOP classes of which we focussed only on the four main classes: 'All alpha (α)', 'All beta (β)', 'Alpha and beta proteins (α+β)' and 'Alpha and beta (α/β)'. The current SCOP database, from February 23 2009, annotates 38221 PDB entries. This is about half the number of PDB entries as of the commencement of this study and so a significant fraction of the target structures was uncategorized. The number of proteins belonging to the SCOP classes varies according to the number of residues in the protein (Figure 1b). Very small proteins of 50 or fewer residues do not belong to any of the four SCOP classes under consideration. Proteins in the moderate size range are uniformly distributed across the SCOP classes.

2.2. Model structures

A BLAST search (Altschul & Lipman, 1990) for homologous PDB structures was done using each target sequence. The searches were performed using an in-house BLAST server with a local copy of the non-redundant PDB. The BLAST searches used the *blastp* algorithm with the *BLOSUM62* matrix. To ensure that all matches between sequences were recorded the number of sequences to show alignments for was set to 20000 and the expectation value set to a large value (1000). The BLAST algorithm works by scoring local alignments (i.e. subsequences) between structures and gives higher sequence identities than global alignments. Sequence identities were therefore recalculated with ClustalW (Thompson *et al.*, 1994), which maximises global sequence alignment. The sequence identity was taken as the fraction of identical residues in the total alignment length. Sequences with

sequence identities below 15% and above 60% were excluded. This is the range of sequence identity that is of interest for this study since above 60% MR rarely fails and below 15% MR rarely succeeds. The structures corresponding to these PDB codes were pruned and edited using the program *Sculptor* (Bunkóczi & Read, 2011) using the default protocol. On average, 8 MR models were found per target. The composition of the database with regards to number of models per target is shown in Figure 1c.

2.3. Templates

For each model and target pair, a transformation to superimpose the model onto the target was determined. An initial superposition with *SSM* (Krissinel & Henrick, 2004) was followed by rigid-body refinement with *Phaser* to find the six-dimensional global LLG maximum. Potential solutions obtained from MR were analysed with respect to this transformation, accounting for symmetry operations and allowed origin shifts, to identify the correct solutions.

3. Results

In total 21822 MR calculations were analysed to find those that succeeded and those that failed. The translation function Z-score (TFZ) for the top peak in the search was found to be a reliable indicator of successful MR, at least for this class of cases where there is one molecule in the asymmetric unit. Z-scores measure the number of standard deviations over the mean. The mean and standard deviation for the translation function search were taken from a random sample of 500 positions for the model in the same orientation. Note that there can be additional incorrect peaks in a translation search, lower than the top peak but still with a non-random TFZ. These usually arise from solutions that are partially correct, such as translations that place a molecule correctly relative to one symmetry axis but not relative to perpendicular axes; such solutions give a better than random prediction of the data.

The placement of the only/first model in polar space groups is ambiguous in the direction of the polar axis. In space group P1, the placement of the first/only model is redundant. In non-polar space groups a peak TFZ of 8 or more indicated a successful solution, while in polar space groups a peak TFZ of 6 was sufficient. Approximately half the solutions with a TFZ of 6.5 were correct in non-polar space groups. While correct solutions could be found with TFZ values as low as 5, they were not necessarily the top peak and it was not clear *a priori* that these solutions are correct. The ratio of correct to total number of solutions by TFZ is shown in Figure 2.

We anticipate that the top TFZ criterion will also apply to searches for subsequent components, which will be tested in future studies. However, it should be noted that the presence of translational non-crystallographic symmetry (tNCS) is a complication. If no account is taken of the effect of tNCS, adding a second molecule in the same orientation as the first one in even an incorrect solution will give a high LLG and TFZ score, for a translation that separates the two molecules by a vector

corresponding to the major off-origin peak in the Patterson map. Fortunately, this artefact can be eliminated by a tNCS correction (McCoy & Read, unpublished), based on a statistical understanding of the effects of tNCS (Read *et al.*, 2013).

3.1. Dependence on sequence identity

Of the 21822 MR calculations, 10921 yielded correct solutions, for which the *VRMS* refinement gives useful results for further analysis. Figure 3a shows a scatter plot of *VRMS* versus sequence identity for correct MR solutions. The distribution of *VRMS* values deviates significantly from the estimate of *eRMSD* in (5). In general the *VRMS* is overestimated by (5) particularly at low sequence identities. This can be explained in part by the implicit selection of models that are sufficiently good to succeed in MR for the analysed subset. However, the distribution of refined *VRMS* about its mean when plotted by sequence identity alone (Figure 3a) is broad.

3.2. Dependence on number of residues

Figures 3b and 3c show scatter plots of *VRMS* values for the data separated into bins by numbers of residues. The distribution about the mean value is significantly narrower when the data are binned in this way. It is evident that the more residues in the model, the better the Chothia & Lesk e*RMSD* agrees with the *VRMS* values. Note that the overall results in Figure 3a are biased towards small structures, which are seen more frequently in the database (Figure 1). The number of residues is therefore a significant second variable in the *VRMS* estimation.

3.3. Estimate of *VRMS*

The functional form of the equation with which to fit the refined *VRMS* with sequence identity and number of residues as parameters was chosen to fulfil a number of limiting conditions. Firstly, the equation was required to increase monotonically. Secondly, for any particular size of protein (measured by number of residues) the equation was required to adopt the functional form of the Chothia & Lesk formula. Thirdly, the increase in estimated *VRMS* was made dependent on the overall linear dimensions of a protein by taking the cube root of a linear function of the number of residues in the model, which assumes that proteins have similar shapes. The functional form for estimated *VRMS* (*eVRMS*) was therefore taken as

$$eVRMS = A(B + N_{res})^{1/3}\exp[C\ H] \qquad (6)$$

where N_{res} is the number of residues in the model and *H* is, as in (5), the fraction of mutated residues. A fit of the parameters *A*, *B* and *C* to the 10921 *VRMS* values of the correct MR solutions was carried out in Mathematica (Wolfram Research Inc., 2010) and produced

$$A = 0.0569, B = 173, C = 1.52$$

This constitutes a two dimensional surface, which is shown in Figure 4a. The mean residual of the Chothia & Lesk eRMSD to all data points is 0.269Å whereas with the fit using (6) it is 0.160Å. *eVRMS* deviates most from the Chothia & Lesk *RMSD* at low sequence identity and for proteins up to 500 residues in length.

In contrast to the earlier implementation of e*RMSD* (5) using the Chothia & Lesk equation (4), we have not applied a lower bound for the *eVRMS* in (6) for two reasons. Firstly, if the *eVRMS* estimate is too low, the model is still likely to be very good so that MR will usually succeed, and a negative LLG at the end of MR, previously associated with low initial estimates of the *RMSD*, is now avoided by *VRMS* refinement as the final step in MR in Phaser. Secondly, the previous lower bound of 0.8Å was too pessimistic when searching with precise models comprising fewer than 50 residues, such as helices in the Arcimboldo procedure (Rodríguez *et al.*, 2009).

The significant scatter of *VRMS* values above and below the *eVRMS* surface indicates that inflating or deflating the *VRMS* estimate may be required in difficult cases. To determine the appropriate sampling distance a histogram of the ratio of *VRMS* to *eVRMS* values is shown in Figure 5a, based on the assumption that the width of the distribution of *VRMS* values is proportional to the mean. The histogram is seen to be approximately Gaussian with a standard deviation of $\sigma_{(VRMS/eVRMS)} = 0.1965$. This lets us define surfaces in steps of $\sigma_{(VRMS/eVRMS)}$ from (6) by simple multiplication of *eVRMS* by a fractional difference as illustrated in Figure 4b.

3.4. Test of *VRMS* estimate

To test how well the VRMS estimate in (6) affects the success rate in MR calculations we re-evaluated a subset of 3375 borderline cases from our MR database, using the new *RMSD* estimates computed with (6). We define borderline cases as those MR calculations for which the template MR solution yields an LLG value within the interval of [20;90] as well as having a global map correlation between the electron densities of the MR solution and the target greater than 0.2. MR problems that do not belong to this set almost always pose little challenge to solve (LLG over 90) or have no credible solution at all (LLG below 20 or map correlation below 0.2). Preliminary calculations with the proposed *RMSD* estimate showed clear gains in TFZ values for easy MR problems. It is, however, the borderline cases that matter in practice. TFZ values improve somewhat in calculations that use (6) rather than (5). For this set of calculations we found the average values shown in Table 1. While the average TFZ increase between the Chothia & Lesk e*RMSD* in (5) and the new *eVRMS* in (6) appears small it should be remembered that the *VRMS* values used for the calculation of *eVRMS* were not limited to the borderline cases only. They also included values for MR calculations where the correct solutions are found with high TFZ.

The $\sigma_{(VRMS/eVRMS)}$ was used to calibrate the perturbation of the *VRMS* to sample above and below the *eVRMS*. In Table 2 the numbers of solved borderline cases are shown for *eVRMS* and *VRMS* estimates perturbed in steps of $\pm$½$\sigma_{(VRMS/eVRMS)}$ and $\pm 1\sigma_{(VRMS/eVRMS)}$. The total number of MR trials that can be solved with at least one of the five estimates is 3036, or 89.8% of the borderline cases. The number of trials that can be solved with at least one of the five estimates but not with the Chothia & Lesk e*RMSD* is 259, whereas the number of trials that are only solved with the Chothia & Lesk e*RMSD* is 20. An analysis of these 20 cases shows that they are all represented by points that have refined *VRMS* values well above the *eVRMS* surface in Figure 4a, in the corner (sequence identity <36%, fewer than 280 residues) where the Chothia & Lesk e*RMSD* estimate deviates most from the new estimate. The average *eVRMS* is 1.15Å for these 20 cases, while the average refined *VRMS* of 1.53Å is identical to the estimate from (5). MR solutions for 12 out of these 20 cases can be rescued by extending the exploration of *VRMS* to include $+1.5\sigma_{(VRMS/eVRMS)}$ and a further 5 by extending to include $+2\sigma_{(VRMS/eVRMS)}$. For the 3 remaining cases, the signal in the MR search is very weak even if the search succeeds; in such cases there is a stochastic element to whether or not the correct solution ends up in the reported list of solutions.

When the estimated coordinate error was not perturbed, the best set of results was obtained with the *eVRMS* values (Table 2), which failed to yield solutions for only 594 of the test cases. By perturbing the *eVRMS* with five different estimates, the number of failures was reduced to only 339, which means that about 1/3 of the failed solutions could be rescued.

In these borderline cases where finding the correct solution can depend on using the right *VRMS* estimate, Phaser frequently reports more than one plausible solution with a TFZ less than 8; the correct solution is not necessarily at the top of the list so it could not be identified with confidence. Nonetheless, these solutions could be used as candidates in the recently developed MR-Rosetta procedure (DiMaio *et al.*, 2011), which has been shown to yield a 50% success rate for further model building based on MR solutions with poor TFZ scores. Likewise these solutions could also be used as a starting point for the morphing procedure (Terwilliger *et al.*, 2012).

3.5. Dependence on SCOP class

We also investigated any dependence of *VRMS* on SCOP class. Figure 5b shows the distributions of *VRMS/eVRMS* values for the 4 SCOP classes of moderate sized proteins under consideration in this study. From these distributions we can deduce the means and standard deviations listed in Table 3.

Proteins belonging to the “All beta” class have the *VRMS* overestimated by about 5% on average whereas “All alpha” proteins are underestimated by about 9% on average. This suggests that the overall folds for proteins dominated by beta sheets are better conserved than those composed of alpha helices. Apart from the “All alpha” class, which is more variable, the standard deviations show that

the distributions separated into fold categories are slightly narrower than the total distribution that combines all fold categories. However, this analysis has not been used to further refine estimates of *VRMS* based on fold class in Phaser because there is still a very large overlap among the distributions for different fold classes compared with the standard deviations of the distributions, and hence it is likely that little would be gained compared to sampling the estimates of the *VRMS* in fractions of $\sigma_{(VRMS/eVRMS)}$. At the same time there would be much added complication in determining and passing information about the fold class to Phaser.

4. Discussion

By using the new *eVRMS* in (6) instead of the Chothia & Lesk e*RMSD* in (5), we have achieved a better estimate of the *RMSD* for use in maximum likelihood MR. This is partly because of the addition of a size dependence, which accounts for the fact that homologous large structures have long range structural perturbations (for example, twists or small hinge motions) that inflate the *RMSD* over the *RMSD* commonly found in homologous smaller structures, and partly because the Chothia & Lesk formula was not designed to provide an effective *VRMS* for MR calculations. The new *eVRMS* increases the success rate with *Phaser* for borderline MR problems. This is therefore now the default setting in *Phaser* for estimating the *VRMS* for an MR model with respect to the unknown target structure.

The new *eVRMS* provides a good overall fit to the mean of the refined *VRMS* values, but there is significant spread about the mean. In cases where a clear solution is not found using the estimated *eVRMS*, additional trials should be carried out using higher and lower estimated values consistent with the observed spread. Our database of test cases also enabled us to estimate the standard deviation of this spread about the mean and hence useful sampling distances above and below the mean. Such a procedure would rescue the cases where the MR search failed with the new *RMSD* values but succeeded with the previous Chothia & Lesk *eRMSD* estimates. An option to inflate or deflate the default *RMSD* estimate by one sigma above and below the mean has been implemented in Phaser, but a broader and finer exploration of this parameter could increase success in pipelines, particularly when following MR with automated rebuilding tools.

To determine sequence identity, we have used ClustalW, in part because this is a tool readily available to users of *Phaser*. One might expect that more sophisticated tools such as HHpred (Söding *et al.*, 2005) would yield more precise estimates of the sequence identity between structurally-aligned residues. However, a control experiment (results not shown) demonstrated that this is unlikely to yield improvements in the quality of *eVRMS* estimates. We repeated the curve-fitting of *VRMS* as a function of sequence identity and model size, but using sequence identities obtained by structural

alignment, and we found that the proportional error in the *eVRMS* estimates was equivalent to that obtained using ClustalW alignments.

We have followed Chothia and Lesk in basing estimated *RMSD* on sequence identity, largely because this is an easy parameter for users of *Phaser* to provide. Nonetheless, there could be advantages to using more subtle measures of sequence similarity. Below 30% sequence identity, it has been shown that the expectation values produced by tools such as BLAST are better correlated than sequence identity with the *RMSD* value between structures (Wilson *et al.*, 2000). Incorporating such a measure instead of, or in addition to, the sequence identity, may be valuable for improving the *eVRMS* estimates in future work.

5. Availability

All methods described are implemented in *Phaser-2.5.4*. *Phaser* is available through the *CCP4* http://www.ccp4.ac.uk; (Winn *et al.*, 2011) and *Phenix* http://www.phenix-online.org; (Adams *et al.*, 2002) software distributions. *Phaser* documentation is at http://www.phaser.cimr.cam.ac.uk

Acknowledgements We are grateful to Nikol Simecek for bioinformatics computing support. This work was funded by NIH grant number GM063210. RJR is supported by a Principal Research Fellowship award from the Wellcome Trust (grant number 082961/Z/07/Z), and this work was facilitated by a Wellcome Trust Strategic Award to the Cambridge Institute for Medical Research.

References

Adams, P.D., Grosse-Kunstleve, R.W., Hung, L.-W., Ioerger, T.R., McCoy, A.J., Moriarty, N.W., Read, R.J., Sacchettini, J.C., Sauter, N.K. & Terwilliger, T.C. (2002). *Acta Cryst. D*, **58**, 1948-1954.

Altschul, S.F. & Lipman, D.J. (1990). *Proc Natl Acad Sci U S A.*, **87**, 5509-5513.

Bunkóczi, G. & Read, R.J. (2011). *Acta Cryst. D*, **67**, 303–312.

Chothia, C. & Lesk, A.M. (1986). *The EMBO Journal*, **5**, 823–826.

DiMaio, F., Terwilliger, T.C., Read, R.J., Wlodawer, A., Overdorfer, G., Wagner, U., Valkov, E., Alon, A., Fass, D., Axelrod, H.L., Das, D., Vorobiev, S.M., Iwai, H., Pokkuluri, P.R. & Baker, D. (2011). *Nature*, **473**, 540-543.

Krissinel, E. & Henrick, K. (2004). *Acta Cryst. D*, **60**, 2256-2268.

McCoy, A.J., Grosse-Kunstleve, R.W.G., Adams, P.D., Winn, M.D., Storoni, L.C. & Read, R.J. (2007). *Acta Cryst D*, **40**, 658-674.

Murzin, A.G., Brenner, S.E., Hubbard, T. & Chothia, C. (1995). *J. Mol. Biol.*, **247**, 536-540.

Read, R.J. (1986). *Acta Cryst A*, **42**, 140–149.

Read, R.J. (2001). *Acta Cryst. D*, **57**, 1373-1382.

Read, R.J., Adams, P.D. & McCoy, A.J. (2013). *Acta Cryst. D,* **69**, 176-183.

Rodríguez, D.D., Grosse, C., González, C., de Ilarduya, I.M., Becker, S., Sheldrick, G.M. & Usón, I. (2009). *Nat. Methods*, **6**, 651-653.

Rossmann, M.G. & Blow, D.M. (1962). *Acta Cryst.*, **15**, 24-31.

Söding, J., Biegert, A. & Lupas, A.N. (2005). *Nucleic Acids Res.*, **33**, W244--W248.

Srinivasan, R. & Ramachandran, G.N. (1966). *Acta Cryst.*, **20**, 570–571.

Terwilliger, T.C., Read, R.J., Adams, P.D., Brunger, A.T., Afonine, P.V., Grosse-Kunstleve, R.W. & Hung, L.W. (2012). *Acta Cryst. D*, **68**, 861-870.

Thompson, J.D., Higgins, D.G. & Gibson, T.J. (1994). *Nucleic Acids Res.*, **22**, 4673-4680.

Wilson, C.A., Kreychman, J. & Gerstein, M. (2000). *J. Mol. Biol*, 233-249.

Winn, M.D., Ballard, C.C., Cowtan, K.D., Dodson, E.J., Emsley, P., Evans, P.R., Keegan, R.M., Krissinel, E.B., Leslie, A.G.W., McCoy, A., McNicholas, S.J., Murshudov, G.N., Pannu, N.S., Potterton, E.A., Powell, H.R., Read, R.J., Vagin, A. & Wilson, K. (2011). *Acta Cryst. D*, **67**, 235-242.

Wolfram Research Inc. (2010). *Mathematica*, 80th edition, Champaign, Illinois: Wolfram Research, Inc.

Table 1 Average Translation Function Z-scores (TFZ) for 3375 cases for the *VRMS* estimates derived from the Chothia & Lesk e*RMSD* as given by (5) and the *eVRMS* given by (6) and perturbed by $\sigma_{(VRMS/eVRMS)}$ values where $eVRMS_{\pm n\sigma} = eVRMS \cdot \left(1 \pm n\,\sigma_{VRMS/eVRMS}\right)$

Chothia & Lesk e*RMSD*	$eVRMS_{-1\sigma}$	$eVRMS_{-½\sigma}$	*eVRMS*	$eVRMS_{+½\sigma}$	$eVRMS_{+1\sigma}$
<TFZ>= 6.28	<TFZ>=6.37	<TFZ>=6.47	<TFZ>=6.48	<TFZ>=6.43	<TFZ>=6.34

Table 2 Matrix of results from 3375 borderline cases solved with the five different estimates of the *VRMS* against cases not solved with the five different estimates where $eVRMS_{\pm n\sigma} = eVRMS \cdot \left(1 \pm n\,\sigma_{VRMS/eVRMS}\right)$. Diagonal elements are total number of solved calculations of the borderline cases with a particular estimate. Off-diagonal values are number of calculations solved with the i-th estimate (row) that cannot be solved with the j-th estimate (column).

Not solved \ Solved	$eVRMS_{+1\sigma}$	$eVRMS_{+½\sigma}$	*eVRMS*	$eVRMS_{-½\sigma}$	$eVRMS_{-1\sigma}$	Chothia&Lesk
$eVRMS_{+1\sigma}$	2840	80	123	139	151	63
$eVRMS_{+½\sigma}$	57	2863	74	95	111	81
eVRMS	92	66	2871	64	85	82
$eVRMS_{-½\sigma}$	122	101	78	2857	45	133
$eVRMS_{-1\sigma}$	171	154	136	82	2820	182
Chothia & Lesk eRMSD	105	146	155	192	204	2798

Table 3 Mean and standard deviation of ratios of *VRMS* to *eVRMS* as a function of SCOP class. The results for total 4 SCOP classes include only proteins for which a SCOP class was assigned.

	All alpha	All beta	Alpha+beta	Alpha/Beta	Total 4 SCOP classes
VRMS/eVRMS	1.089	0.946	0.990	1.019	0.997
$\sigma_{(VRMS/eVRMS)}$	0.187	0.167	0.157	0.168	0.172

a)

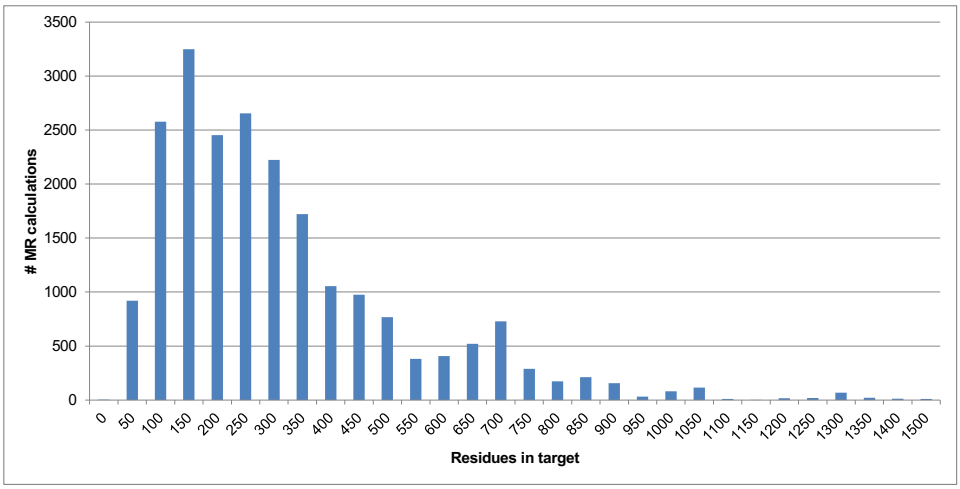

b)

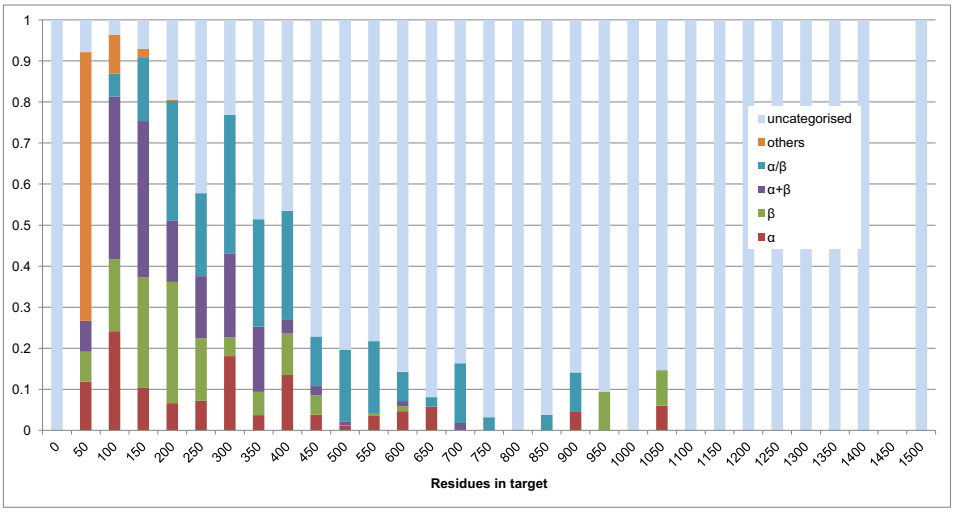

c)

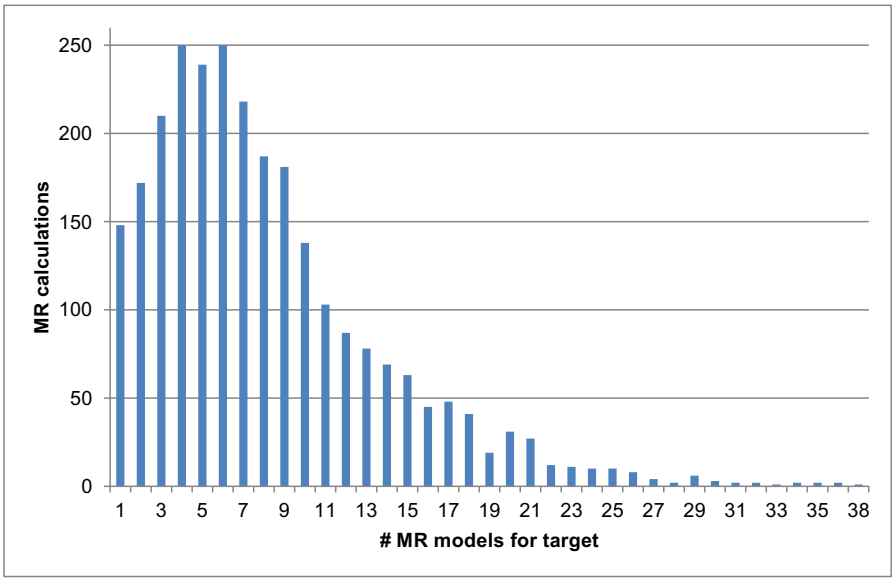

Figure 1 (a) Number of MR calculations as a function of number of residues in their respective MR targets. (b) Fraction of MR calculations with target belonging to certain SCOP classes as a function of number of residues in target. (c) Histogram of number of MR models used for MR calculations.

a)

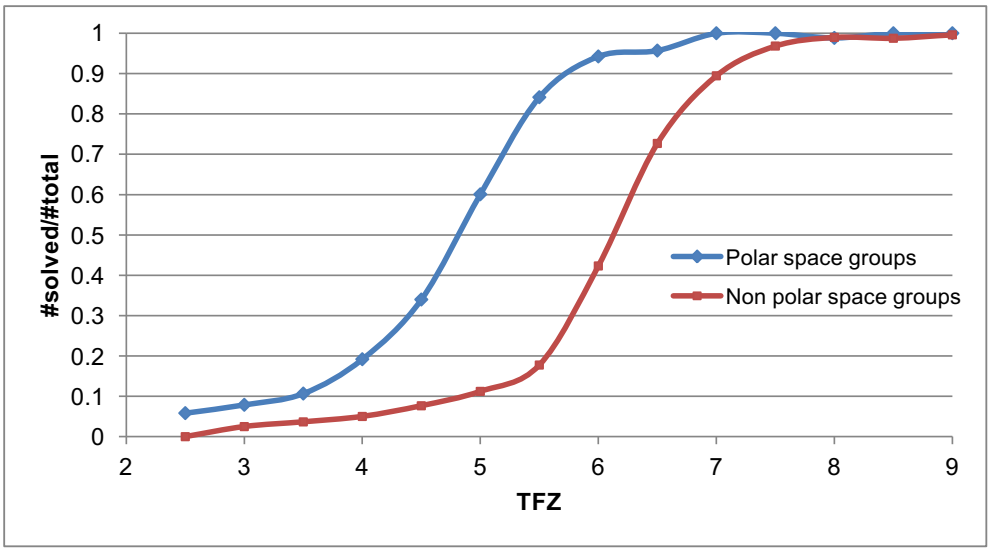

b)

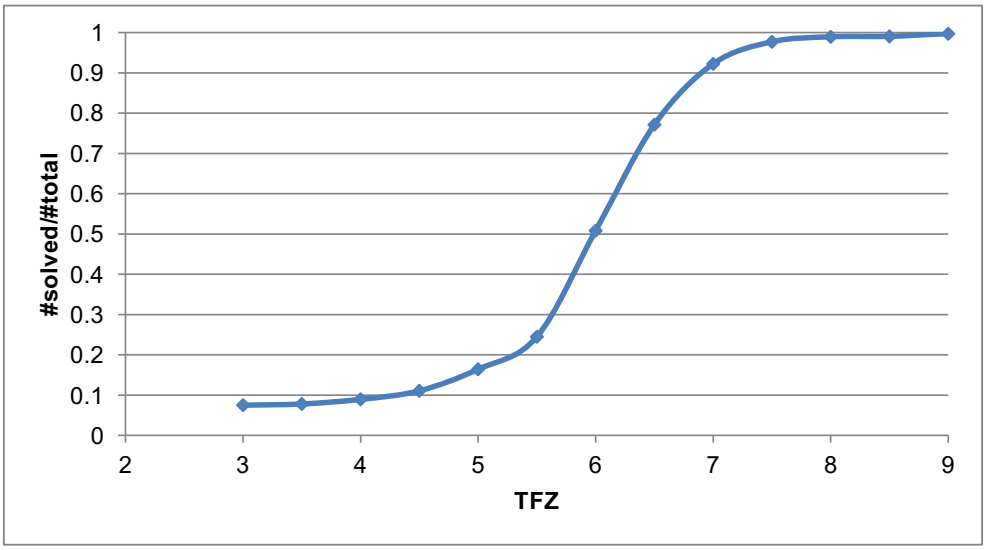

Figure 2 Fraction of correct placements of the only/first component in the asymmetric unit as a function of TFZ by polar and non-polar space group. Polar space groups accounted for one quarter of the test cases in our database, while the 1% of test cases that were in space group P1 were excluded from this analysis.

a)

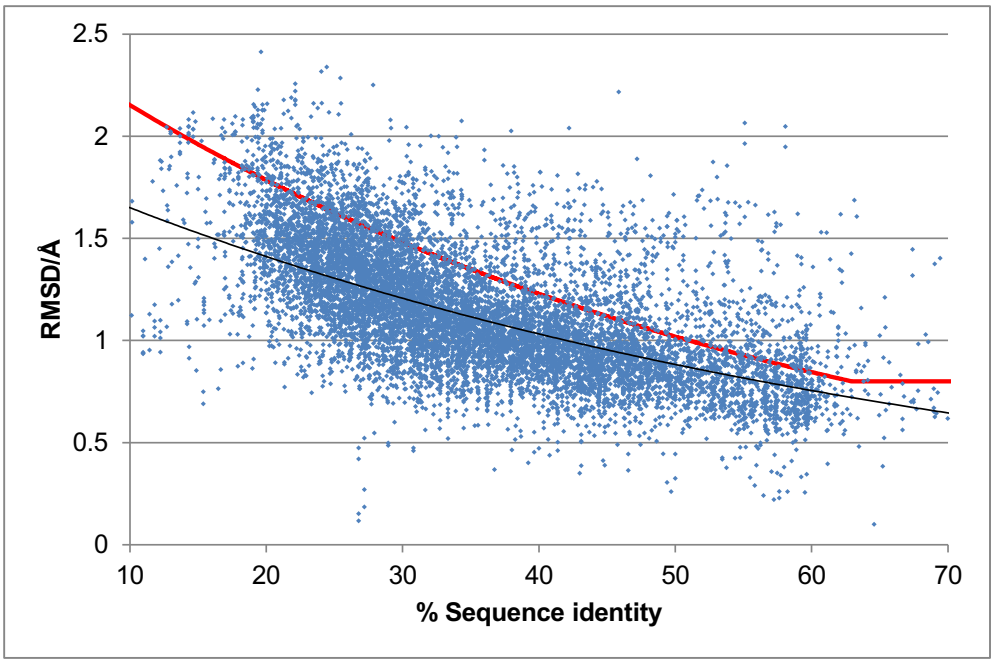

b)

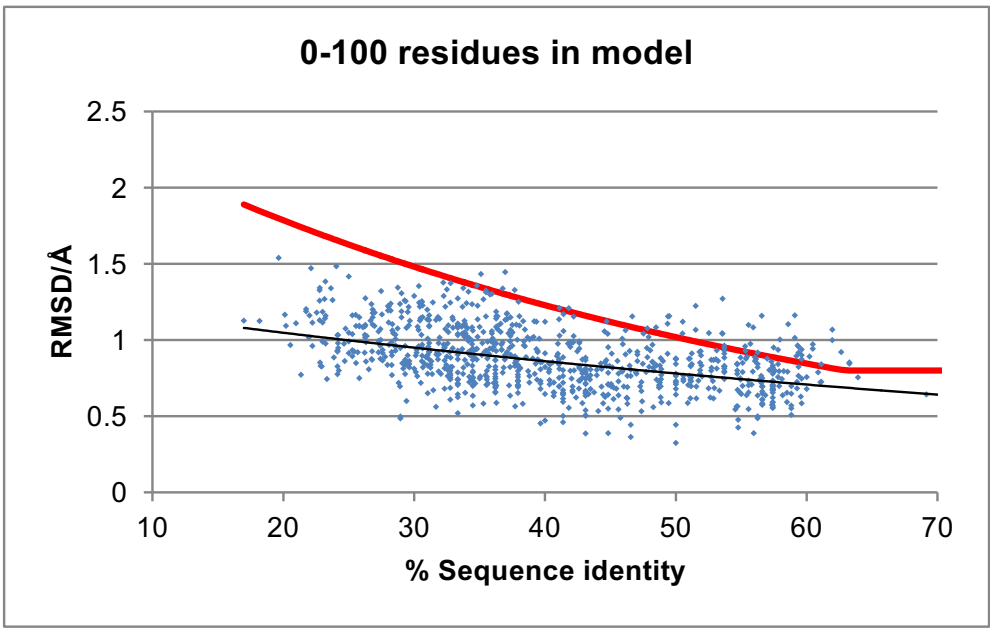

Figure 3 Scatter plot of *VRMS* against sequence identity for correct MR solutions, 10921 data points. Red line represents (5) in *Phaser*. (a) all data (b) data for models less than 100 residues (c) data for models of between 100 and 500 residues.

a)

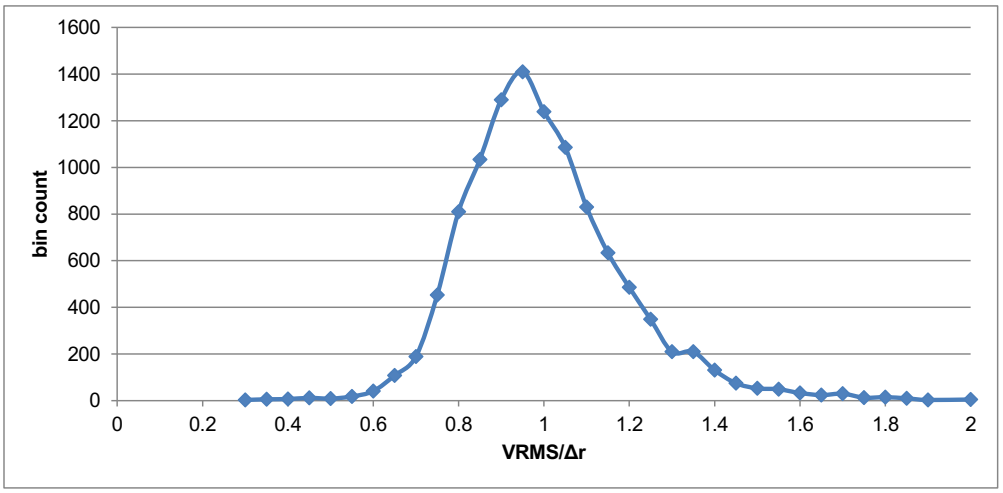

b)

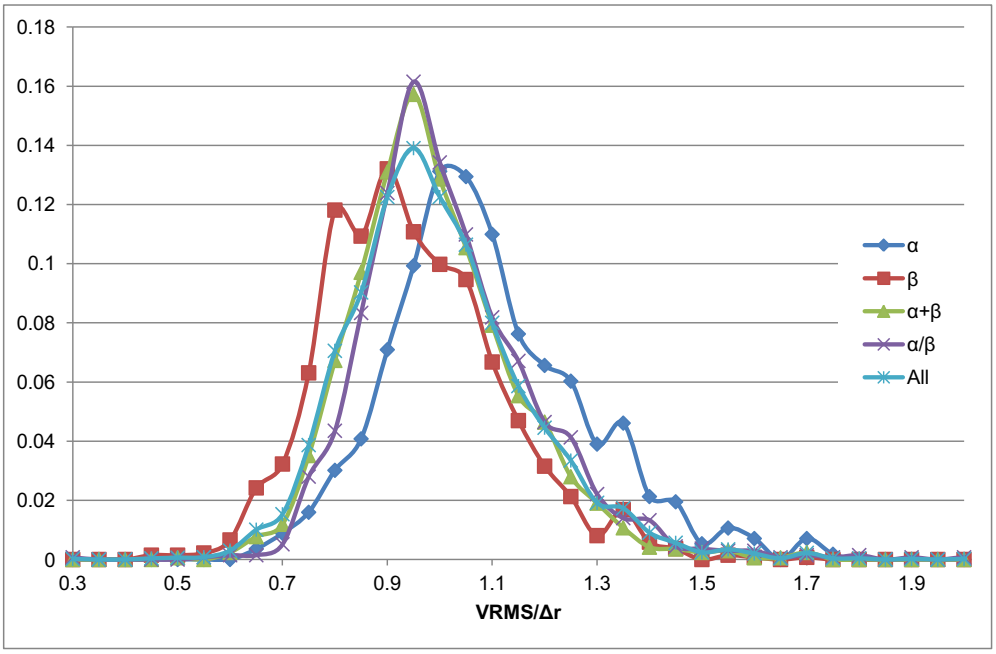

Figure 4 (a) Fit of the *eVRMS* (light blue surface) and Chothia & Lesk *RMSD* in (4) (pale yellow surface) to the refined *VRMS* values of 10921 MR solutions. The effective limits of *eVRMS*(sequence identity,number of residues) are *eVRMS*(100%,15) = 0.362 Å and *eVRMS*(15%,1500) = 2.53 Å (b) Fit of the *eVRMS* (light blue surface) and *eVRMS* ±1σ surfaces to the refined *VRMS* values of 10921 MR solutions.

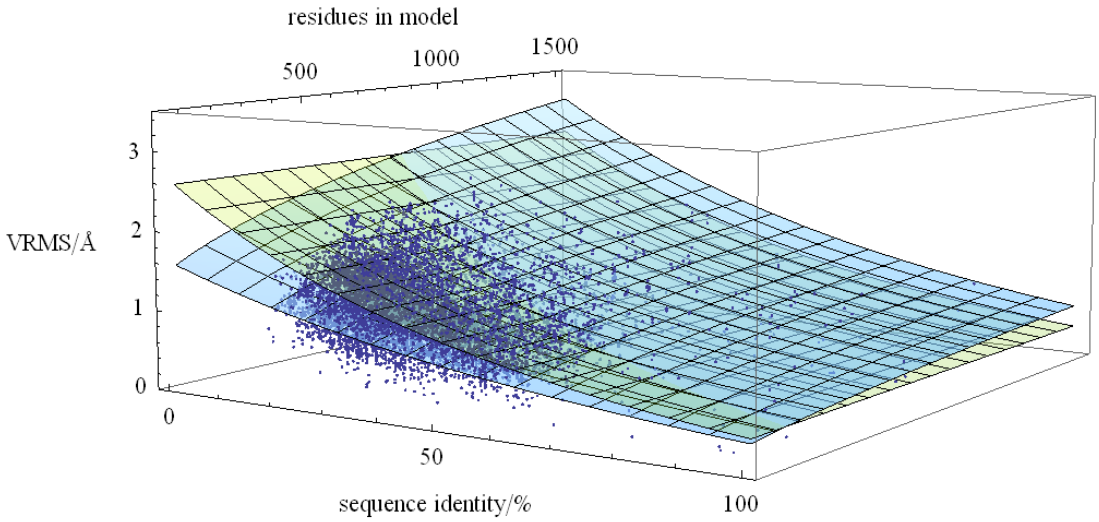

a)

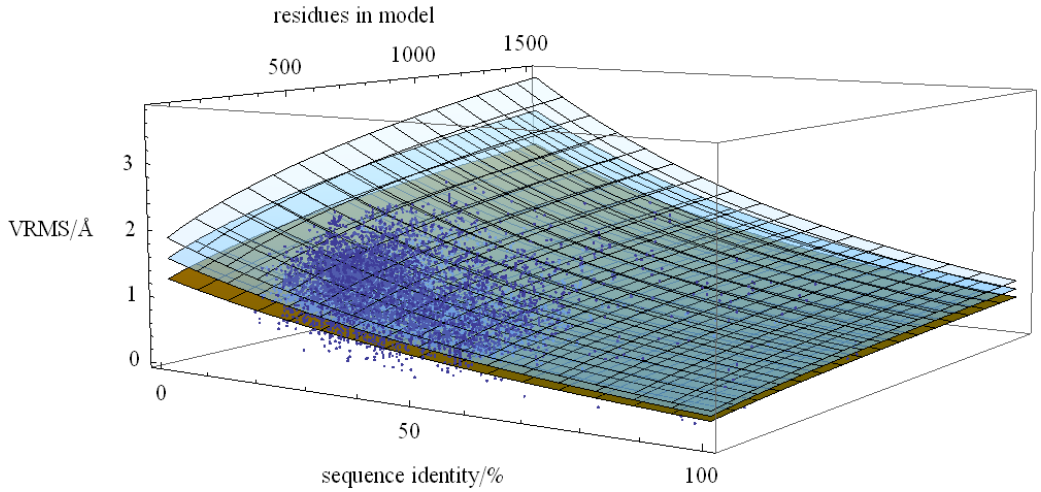

b)

Figure 5 (a) Histogram of *VRMS*/*eVRMS* for the 10921 correct solutions in the MR database. The distribution is approximately Gaussian (b) Frequency distribution of *VRMS*/*eVRMS* for the 4 major SCOP classes, computed for models ranging from 100 to 300 residues in length.